Tropical Ocean Circulation Experiments

MOJIB LATIF

Max-Planck-Institut für Meteorologie, D 2000 Hamburg 13, FRG

(Manuscript received 17 July 1985, in final form 4 September 1986)

ABSTRACT

A primitive equation model of the equatorial Pacific Ocean was forced by realistic wind stress distributions over decades. Results were presented for a set of two experiments. In the first experiment the model was forced by an objectively analyzed wind field, while for the second experiment a subjectively analyzed wind field was used. The results indicate a strong sensitivity of the model to the choice of the wind field. Especially, model results in the eastern Pacific show big differences between the two model runs.

Taking the results of the second model run the performance of the model with respect to interannual variability is investigated. Sea level, temperature and zonal currents show pronounced interannual variations within the equatorial belt from 10°N to 10°S.

Special attention is given to the simulation of the 1982/83 El Niño event. The model reproduces most of the basic features, which were observed during this El Niño event. In particular the deceleration of the equatorial undercurrent, the evolution of eastward surface currents and the zonal redistribution of heat associated with an eastward propagation of warm water are simulated by the model.

1. Introduction

The equatorial Pacific Ocean exhibits the most prominent interannual signal of climate variability known as El Niño. During these events warm surface waters appear for several months over the entire equatorial zone. The relation of the phenomenon to the wind anomaly field has clearly been revealed (Wyrtki, 1975) but also the imbedding of the El Niños in global interannual climate variations has been demonstrated by the connection to the Southern Oscillation (e.g., Wright, 1977) and to teleconnections to North American weather indices (e.g., Horel and Wallace, 1981). Apparently, modeling the Pacific Ocean circulation is an essential prerequisite for understanding and eventually predicting this part of global climate variability. A major step in this task was the clear attribution of observed sea level variations to equatorially trapped waves forced by realistic wind anomalies (Busalacchi and O'Brien, 1981; Cane, 1984), a piece of work which was the logical consequence of a series of equatorial wave process studies as those of Hurlbert et al. (1976), McCreary (1976) and Cane (1979a,b). However, those models do not include thermodynamic processes and these are necessary ingredients to predict sea surface temperature which is the essential parameter in air-sea interaction studies. There is a range of models designed for this purpose where high-resolution, general circulation models represent the highest degree of complexity. In this paper we present an investigation of the response of such a model to realistic wind forcing. High resolution oceanic models have traditionally been used to study the mean state of the ocean circulation. In the equatorial region, however, the wind forcing is highly variable on time scales comparable with the intrinsic oceanic time scales so that the oceanic adjustment cycles to changing winds appear as relevant to study as the asymptotic mean state of the circulation. Philander has investigated the response of an equatorial ocean general circulation model (OGCM) to abruptly and periodically changing winds in a series of papers (Philander and Pakanowski, 1980, 1981; Philander, 1981) and has revealed the importance of nonlinear advective effects in addition to the wave processes for the response of the upper ocean. Simulations of the seasonal cycle of the tropical Atlantic Ocean as well as the 1982/83 El Niño event have been performed (Philander and Seigel, 1985) and have clearly demonstrated the ability of OGCMs to reproduce the observed variations of the thermal and velocity structure of the equatorial ocean in response to the actual wind.

The numerical model used in the present study differs slightly from the model used by Philander. The dimensions of the model are those of the equatorial Pacific. We use variable resolution in all three directions.

Experiments were performed by using two differently analyzed wind fields. In the first case, the model was forced by winds which result from an objective analysis of the Wyrtki and Meyers dataset (Wyrtki and Meyers, 1975a,b), while in the second case, winds from a subjective analysis of the same dataset were used. The duration of both experiments is of the order of decades. There are 18 common years of integration which can be compared directly. Only results from the second

experiment were used to study the interannual variability and the evolution of 1982/83 El Niño event.

In section 2 the ocean model is described. The wind fields are presented in section 3, while the experimental design and the model results are shown in sections 4, 5, 6 and 7. The results are then summarized in section 8.

2. Model

The numerical model is based on the primitive equations with the Boussinesq and hydrostatic approximations on an equatorial β-plane:

$$\mathbf{u}_t + (\mathbf{v}\cdot\nabla)\mathbf{u} + \beta y\mathbf{k}\times\mathbf{u} + \nabla p = A_h\nabla^2\mathbf{u} + (A_v\mathbf{u}_z)_z \quad (2.1)$$

$$\nabla\cdot\mathbf{v} = 0 \quad (2.2)$$

$$T_t + (\mathbf{v}\cdot\nabla)T = (k_vT_z)_z. \quad (2.3)$$

There is no horizontal diffusion of heat in the model because there is no physical or numerical reason to incorporate any horizontal mixing. Moreover, the values of diffusion coefficients are notoriously uncertain.

The pressure is given by

$$p = g\zeta - g\alpha\int_z^0 T dz' \quad (2.4)$$

where ζ is the surface elevation which is not eliminated as in the GFDL-type models (Bryan, 1969) but kept as a prognostic variable calculated from the vertically integrated continuity equation:

$$\zeta_t + \nabla\cdot\int_{-H}^0 \mathbf{u}dz = 0. \quad (2.5)$$

This equation is numerically integrated by an implicit algorithm which damps the surface gravity mode but is neutral to the geostrophic mode. The baroclinic part (2.1) and (2.3) is integrated explicitly with a time step of two hours.

The model ocean is a rectangular box and covers the area from 30°S to 30°N, 150°E to 80°W. In the horizontal as well in the vertical direction the grid spacing is variable: The meridional resolution decreases from 50 km at the equator to about 400 km at the northern and southern boundaries, while the longitudinal resolution is 50 km near the coasts decreasing to 800 km in the center. Vertically there are 13 levels, most of them are placed within the thermocline. The locations of the levels within the upper 300 m can be seen in Fig. 13. Bottom topography is not included so that the ocean floor is at a constant depth of 4000 m.

The vertical eddy viscosity, the horizontal eddy viscosity, and the vertical eddy diffusivity have constant values of 15, 10^8 and 1 in units $cm^2\ s^{-1}$.

The model is forced at the surface by wind stress and heating. The wind fields are described in the next section. The heating is parameterized according to Haney (1971) with a constant forcing temperature of 29°C and a relaxation time of about 30 days.

At the bottom and at lateral boundaries a no-slip condition is used. A no-heat flux condition is applied at the bottom. Since there is no explicit horizontal diffusion of temperature, no further boundary conditions are needed. Notice, however, that with these boundary conditions the model ocean would be thermally isolated at the walls and at the bottom and would continually become warmer due to the choice of the heat flux parameterization. This warming trend can be seen in the first experiment (Fig. 5a). In order to avoid this warming the temperature below 1000 m was fixed at the northern and southern boundaries during the second experiment.

3. Wind data

The two wind fields that were used to force the model are both analysis products of the Wyrtki and Meyers wind dataset. One analysis was done by Barnett (1983). The aim of this work was to produce a dataset which is suitable to study the interactions of the Pacific trade-wind field and the Asian monsoon on interannual time scales. Barnett's analysis is based on the objective technique of empirical orthogonal functions (EOFs), which strongly discriminates against small scale noise. As pointed out by Barnett, from a statistical point of view, only ten EOFs of the wind anomaly field can be classified as signal. The first five EOFs have been included in the reconstruction of the wind anomaly field. These only describe about 45% of the original variance. As will be shown later the filtering is rather strong in the eastern Pacific, while the western Pacific region is less affected.

Barnett's analysis yielded bimonthly wind vectors for the period 1947–1978 in the equatorial strip 30°S–30°N, 35°E–75°W. The annual cycle was subtracted before the EOF analysis was done and it is given on a 2° × 10° grid. Wind anomalies have been smoothed on a 4° × 20° grid. For the equatorial wave guide the zonal wind stress component is the most important forcing mechanism in understanding the thermal response. Figure 1 displays the time series of zonal wind stress anomalies averaged over three different regions from 5°S to 5°N in the eastern, central and western Pacific. Zonal wind stress anomalies exhibit largest amplitudes west of the dateline reaching peak values of about 0.3 dyn cm^{-2}. Notice further the small anomalies in the eastern Pacific. All time series show the predominance of westward anomalies over the entire equatorial Pacific after the El Niño year 1972.

The wind field that was used in the second experiment is based on a subjective analysis by Goldenberg and O'Brien (1981). One of the major goals of this work was to create a dataset which can be used in ocean circulation experiments. The wind data consist of monthly mean values for the period 1961–83. The resolution is 2° × 2°, and the analyzed area extends from 29°N to 29°S and from 124°E to 70°W.

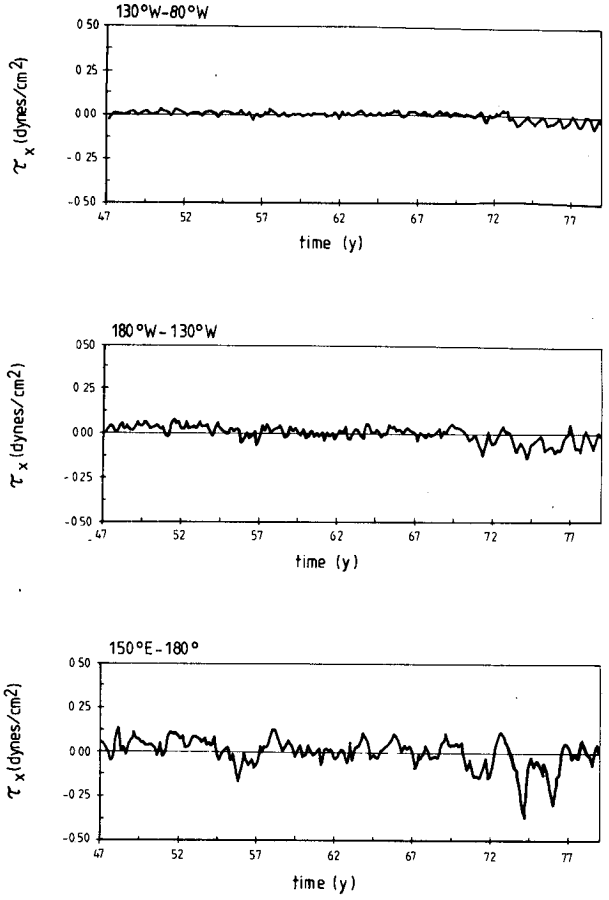

FIG. 1. Time series of zonal wind stress anomalies as calculated from the dataset of Barnett averaged from 5°N to 5°S for (a) eastern Pacific, 130°W–80°W, (b) central Pacific, 180°–130°W and (c) western Pacific 150°E–180°.

In Fig. 2, the time series of zonal wind stress anomalies averaged over the same regions as in Fig. 1 are presented. As can be seen from Figs. 1 and 2 the amplitudes of the zonal wind stress anomalies are much larger in Fig. 2. Notice that the scale in Fig. 1 is half of that in Fig. 2. The reduction of variance in Barnett's dataset is most prominent in the eastern Pacific (Fig. 1a), amplitudes in this region being almost one order of magnitude smaller than in the dataset of Goldenberg and O'Brien. Both datasets exhibit almost linear trends, which are most obvious in the eastern Pacific (Fig. 1a, 2a).

Figures 3a and 3b show variance spectra of zonal wind stress anomalies along the equator calculated from both datasets. For the Barnett dataset (Fig. 3a) three regions of high variance can be found. High variances can be identified at the low frequency end of the spectrum along the entire equator.[1] This maximum is due to the trends in the time series, which are seen in Fig. 1. This region of high variance extends into the western Pacific up to frequencies of about 0.5 cycles per year (cpy). This belt of relatively high variance is associated with the Southern Oscillation phenomenon, which appears to have a peak in this frequency range and to play a major role in the interannual variability of the Pacific Ocean. It has been shown by many authors (e.g., Wyrtki, 1975) that the western and parts of the central Pacific are key regions with respect to the initiation of El Niño. The area west of the dateline is characterized by event like changes of the zonal wind stress (Fig. 1c) and it is therefore a potential region of wave excitation. A third region of high variance is found in the eastern Pacific for frequencies of about 0.9 cpy.

The low frequency characteristics of zonal wind stress anomalies computed from the dataset of Goldenberg and O'Brien are very similar to that shown in Fig. 3a. Both the increase of relative variance at the low frequency end of the spectrum as well as the extention of this area to higher frequencies in the western Pacific are seen in Fig. 3b. The most important difference between the two spectra is the absence of high variance in the eastern Pacific at a period of about 13 months.

Wind stress vectors were calculated by applying a simple drag law with a constant drag coefficient of 1.5 $\times 10^{-3}$ and air density of 1.2 kg m^{-3}. For use in the model these wind stress vectors were then interpolated linearly in space and time.

4. Experimental design

Experiments were performed by using both wind datasets to force the model. The experimental design is given in Fig. 4a. Initial conditions are the same in both experiments. At the beginning the ocean is at rest and has a horizontally uniform stratification, which is shown in Fig. 4b. For convenience, the two experiments are called Barnett and O'Brien case. For both experiments the spinup phase consists of forcing the model with mean winds for one year and with the seasonal cycle for three years. After this spinup phase the model has reached a cyclostationary state in which wave propagation no longer plays an important role. Finally, the model was driven by the full wind forcing. In the Barnett case the integration was carried on for 32 years covering the period from 1947 to 1978, while the O'Brien case consists of 23 years starting in 1961. There are 18 common years of integration, which show how the different features of both datasets project onto the model results.

5. Sensitivity to wind forcing

A major question which may be relevant for the Tropical Ocean Global Atmosphere (TOGA) experiment is the question of accuracy for surface wind observations. The two wind fields used in this study may

[1] The trends were not removed, neither before computing the spectra nor before using the wind stress field as forcing in the ocean model.

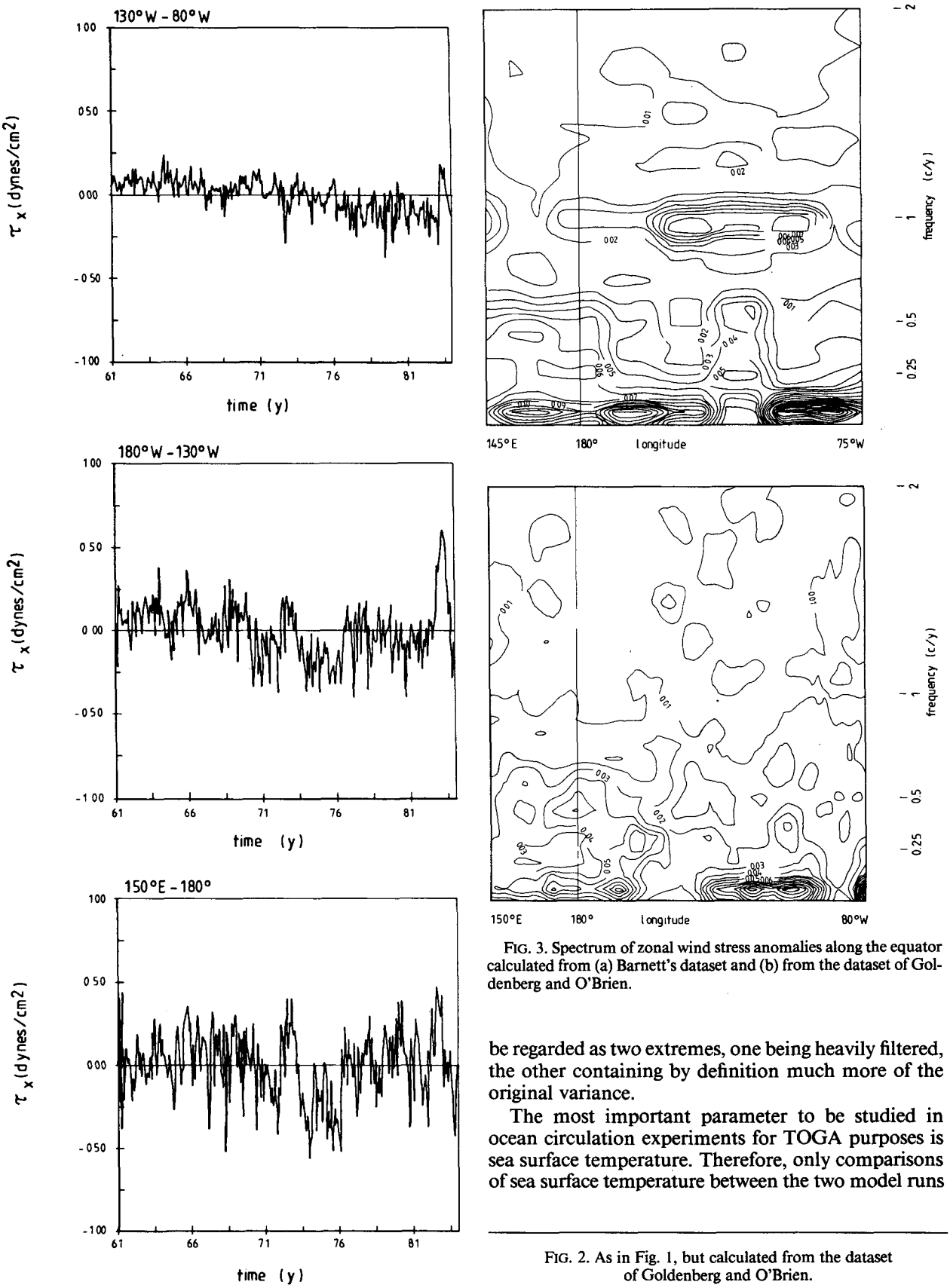

FIG. 3. Spectrum of zonal wind stress anomalies along the equator calculated from (a) Barnett's dataset and (b) from the dataset of Goldenberg and O'Brien.

be regarded as two extremes, one being heavily filtered, the other containing by definition much more of the original variance.

The most important parameter to be studied in ocean circulation experiments for TOGA purposes is sea surface temperature. Therefore, only comparisons of sea surface temperature between the two model runs

FIG. 2. As in Fig. 1, but calculated from the dataset of Goldenberg and O'Brien.

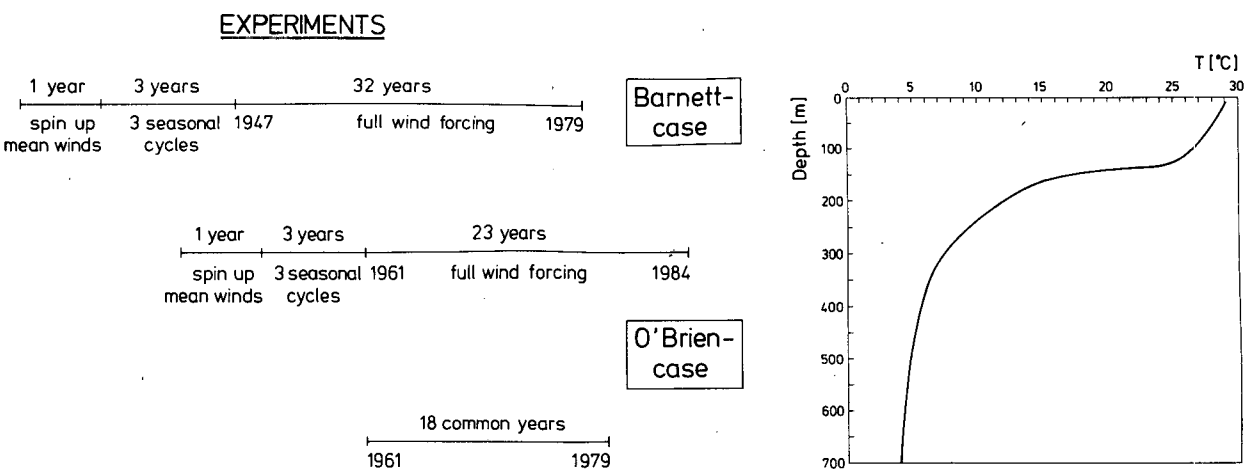

FIG. 4. (a) Schematic representation of the experimental design. (b) Initial temperature field in the upper 700 m of the ocean. Below 700 m temperature decreases linearly to 1°C.

are presented in this chapter. In order to make differences more distinct, the seasonal cycle was removed.

Figure 5 shows simulated sea surface temperature anomalies in the eastern Pacific for the Barnett case as well as for the O'Brien case. As can be seen from Fig. 5a there seems to be no systematic relationship between simulation and observation in the Barnett case. Except for the 1972 El Niño event, warm events do not occur in this experiment. The variability of sea surface temperature anomalies in the Barnett case is characterized by variations with periods of about 13 months. This result may clearly be attributed to the wind field, which shows high variance for the same period (Figs. 1a, 3a).

The lower panel of Fig. 5 shows the simulation of sea surface temperature anomalies for the O'Brien case.

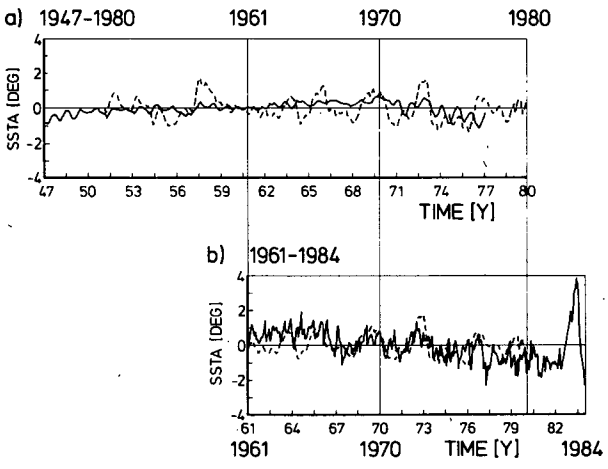

FIG. 5. Time series of observed (dashed) and computed (full line) sea surface temperature anomalies in the eastern Pacific (80°W–140°W) for (a) the Barnett case and (b) the O'Brien case.

In general the type of variability is much better simulated in this case than in the Barnett case. Nevertheless, the increase in described variance is small. While the simulation in the Barnett case accounts for 28% of the observed variance, the simulation in the O'Brien case accounts for 32%. The improvement is best expressed by the coherence spectra (not shown). While the coherence spectrum between the calculated and the observed time series does not show significant peaks for the Barnett case, the coherence spectrum for the O'Brien case exhibits a peak with a value of 0.78 and vanishing phase for periods of about 39 months, the peak being significant on the 95% significance level.

Notice, that both simulations show almost linear trends. In the Barnett case the slow warming trend until 1972 is due to the continuous input of heat at the surface. This warming is discussed in more detail in Latif et al. (1985).

The simulation using the dataset of Goldenberg and O'Brien also shows a trend.[2]

The situation in the western Pacific is shown in Fig. 6. Both simulations are in good agreement with the observed time series of sea surface temperature anomalies. In both simulations all observed warm events as well as the observed cold events are reproduced. While the amplitudes compare remarkably well in the Barnett case, they are systematically overestimated in the O'Brien case. The difference in the amplitudes between the two model runs is due to the different strength of

[2] As was already discussed in section 3 (Fig. 2a), zonal wind stress anomalies in the Eastern Pacific show also an almost linear trend, which is downward. This means that there is an intensification of the westward wind stress over the whole period of integration. It is therefore concluded that the strengthening of the wind stress causes stronger upwelling, which results in a gradual cooling.

zonal wind stress anomalies, which was already discussed in section 3 (Figs. 1c, 2c). For the western Pacific region zonal wind stress anomalies calculated from the dataset of Goldenberg and O'Brien are about two times larger than the anomalies determined from Barnett's dataset.

The correlations between the time series presented in Fig. 6 are 0.82 for the Barnett case and 0.71 for the O'Brien case, while the coherence for periods of about 3 years lies in both cases above a value of 0.9, exceeding in both cases the 99% significance level. The success of the model in reproducing the observed variations of sea surface temperature anomalies in the western Pacific independently from the choice of the wind field suggests that a simple relationship may exist between wind stress and sea surface temperature anomalies. In order to test this hypothesis the simulation was repeated using a simple zero dimensional model for the evolution of sea surface temperature anomalies:

$$\frac{\partial T'}{\partial t} = -C_1 T' + C_2 \tau'_x. \tag{5.1}$$

Equation (5.1) relates the evolution of the temperature anomaly T' within a mixed layer with constant depth to a Newtonian cooling-type heat flux and to the locally forced part of vertical and horizontal advection of heat. Therefore the coefficient C_2 describes the net effect of the two processes. The model (5.1) is fitted to data by prescribing the observed local wind stress anomalies from the dataset of Goldenberg and O'Brien and by minimizing the quadratic error between the model temperature anomalies and the observed temperature anomalies. This procedure yields an optimal model by finding the appropriate coefficients C_1 and C_2.

The main result from this zero-dimensional model is that a large portion of the observed sea surface temperature variability can be explained by such a simple model. For example, the model time series at the dateline can account for 65% of the observed variance. This implies that the western Pacific is a region of strong local forcing. It will be shown later (Fig. 18) by discussing the results of the more sophisticated primitive equation model that all three advective processes contribute to the warming during El Niño events.

These local arguments do not work in the eastern Pacific. The fitting procedure in this region yields time series that do not correlate well with the observations. For a location corresponding to the Galapagos Islands only 19% of the observed variance can be explained by the model 5.1. This result is not surprising, because it is commonly believed that remote forcing is important in the eastern Pacific (e.g., Wyrtki, 1975) in addition to local effects.

In summarizing the results of this section the two experiments demonstrate that the quality of simulation depends strongly on the choice of the wind field. The sensitivity is strongest in the eastern Pacific, while in the western Pacific both simulations show satisfactory agreement with observations. In addition a model with no dynamics [i.e., (5.1)] can reproduce much of the observed sea surface temperature variability in the western Pacific.

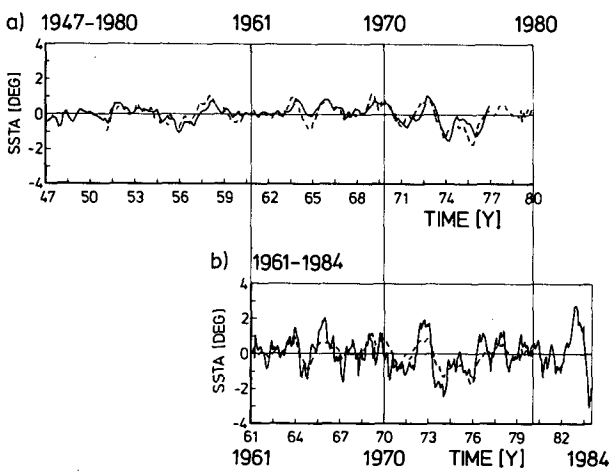

FIG. 6. As in Fig. 5 but for sea surface temperature anomalies in the western Pacific (140°W–150°E).

6. Interannual variability

Guided from the results of the preceding section only results from the O'Brien case were used to study the interannual variability and the evolution of the 1982/83 El Niño event.

As was shown by Busalacchi et al. (1983), interannual sea level variations can successfully be simulated by forcing a linear, reduced gravity model with realistic winds. Since sea level is a prognostic variable in the model presented in this paper [Eq. (2.5)], the investigation of interannual variability is started with sea level. This quantity is in addition the best observed quantity in the equatorial Pacific. Figures 7a and 7b show sea level variations in the eastern and in the western Pacific, for locations corresponding to the Galapagos Islands (Fig. 7a) and Truk Island, respectively. It is seen from Fig. 7a that with respect to low frequency variations the agreement between model and observations is reasonably good. During El Niño events the model shows anomalous high sea level, this feature being most pronounced during the events of 1972 and 1982/83. The amplitudes of this low frequency variations are of the order of 10 cm, which agrees quite well with the observed range. The biggest difference between model and observations is the presence of a linear trend in the model time series, which is absent in the observed curve. The slow fall of sea level in the model must be attributed to the trend in zonal wind stress (Fig. 2a), which prevents the model from reaching a constant mean sea level.

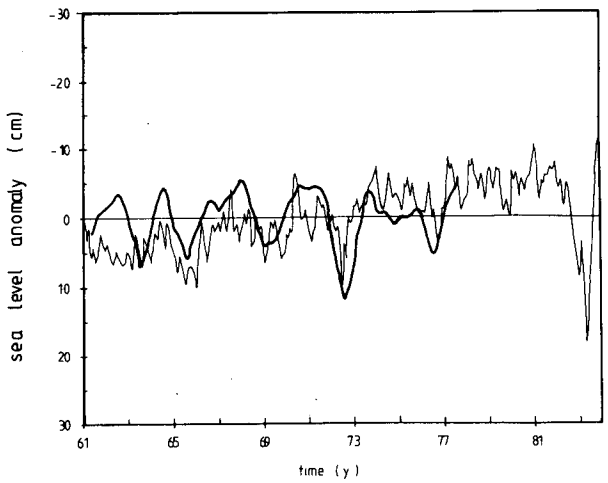

FIG. 7a. Comparison of sea level anomalies for a location corresponding to Galapagos Islands. Observed (thick line) curve is a 12 month running mean taken from Busalacchi et al. (1983), computed (thin line) values are deviations from the seasonal cycle.

The corresponding picture for Truk Island is given in Fig. 7b. For this location the model reproduces not only low frequency variations but also variations on shorter time scales. As can be seen from Fig. 7b, El Niño events are accompanied by lower than normal sea level. The drop in sea level in the western Pacific is of the order of 20 cm for the 1972 and the 1982/83 warm events. Together, Figs. 7a and 7b demonstrate the ability of the model to reproduce the basic features of interannual sea level variability.

As was already pointed out by Busalacchi et al. (1983), interannual sea level variability on the equator can consistently be explained by wave processes. An investigation of lagged cross correlations (not shown) of sea level anomalies along the equator yields a similar result. In the present case it is found that Kelvin waves of the first internal mode play an important role in the sea level response. The phase speed of this wave deduced from model sea level is 2.7 m s^{-1}, which coincides with the theoretical value calculated by solving the eigenvalue problem for the initial stratification.

Figures 8 and 9 show time series of temperature and zonal current anomalies for different locations at 10 and 100 m depth. Temperature anomalies are displayed in Fig. 8. As was already discussed, guided by Figs. 5b and 6b, the surface temperatures on the equator show a pronounced interannual signal associated with warm and cold events. The same type of low frequency variability is found at a depth of 100 m (Figs. 8a, 8b). Temperature anomalies along the southeastern coast show also strong interannual variations (Fig. 8c), which are most pronounced at subsurface levels.

The evolution of zonal current anomalies are shown in Fig. 9. On the equator at 171°W (Fig. 9a) there are found positive current anomalies reaching peak values of 1 m s^{-1}. Except for the anomaly in 1977, strong

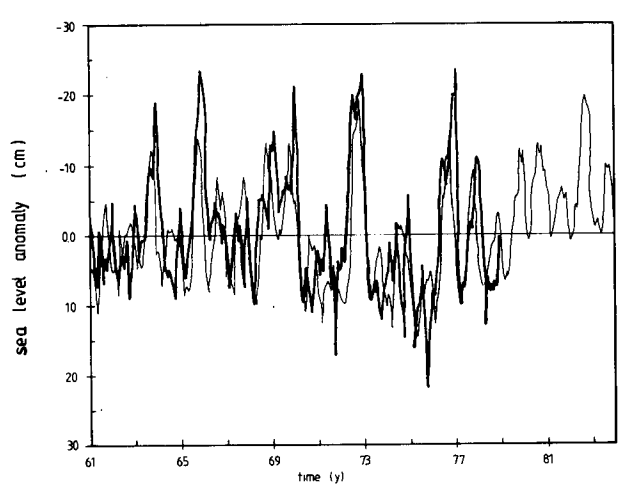

FIG. 7b. Comparisons of sea level anomalies for a location corresponding to Truk Islands. Observed (thick line) curve is taken from Busalacchi et al. (1983), computed values (thin line) are deviations from long term mean sea level.

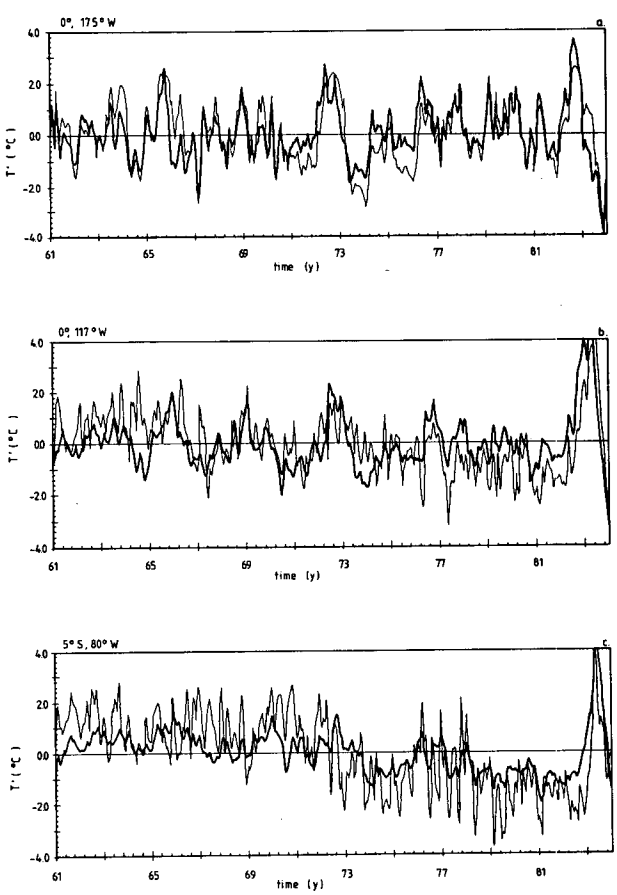

FIG. 8. Computed temperature anomalies at 10 m (thin line) and at 100 m (thick line) depth for (a) 0°, 175°W, (b) 0°, 117°W and (c) 5°S, 80°W.

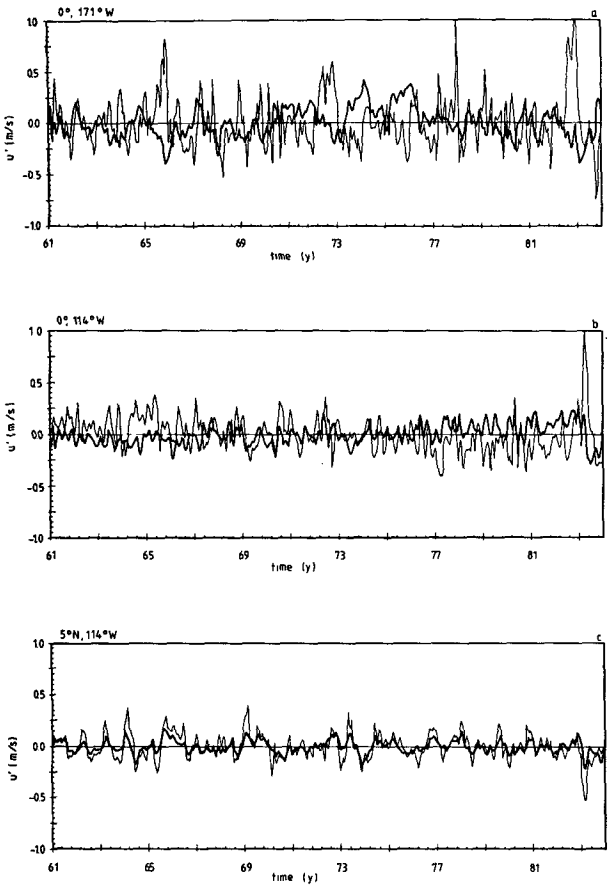

FIG. 9. Computed zonal current anomalies at 10 m (thin line) and 100 m (thick line) depth for (a) 0°, 171°W, (b) 0°, 114°W and (c) 5°N, 114°W.

positive anomalies occur only during El Niño events. As will be shown later, the amplitudes are large enough to reverse the direction of the westward flowing equatorial surface current. During the El Niño event of 1972 the model shows anomalous eastward flow for the entire year 1972, while during the "post El Niño" year 1973 pronounced negative anomalies are found. These results are very similar to the results of Gill (1983), who used sea level records at the eastern boundary to calculate zonal current anomalies in the central Pacific.

As can be seen from Fig. 9a, surface and subsurface currents on the equator behave in an opposite manner. Positive current anomalies at the surface coincide with negative anomalies of the undercurrent some months later and vice versa. The deceleration of the undercurrent is most pronounced during the warm events of 1965, 1972 and 1982/83, while in late 1973, early 1976 and late 1983 large positive anomalies occur during periods when the ocean in this region is anomalously cold (Fig. 8a).

Time series of zonal current anomalies on the equator in the eastern Pacific are shown in Fig. 9b. Except for the 1982/83 El Niño event, variability for this location is weak. During early 1983 surface current anomalies of 1 m s^{-1} can be found. The reduced variability in the eastern Pacific may be partly due to the relatively high resolution in the vicinity of the eastern boundary, which can lead to a stronger damping of the small scales by the horizontal eddy viscosity. Another possible reason for the reduced current variability may be the choice of constant values for the vertical eddy viscosity.

Zonal current anomalies at 5°N, 114°W are presented in Fig. 9c. For this location surface and subsurface currents behave very similarly, indicating barotropic changes. During the El Niño events of 1963, 1965, 1969, 1972 and 1976, enhanced eastward flow is found, resulting in an intensification of the North Equatorial Counter Current. No such intensification can be seen at this grid point during the last El Niño event of 1982/83. As will be shown later (Fig. 15), the intensification of the Counter Current took place at a latitude of about 10°N in September 1982.

Figure 10 shows depth–time sections of temperature and zonal currents on the equator for all 23 years. During the whole period of integration the model shows neither a significant deepening of the thermocline nor a systematic change in the current structure, which demonstrates the stability of the model. As can be seen from these sections current changes (Figs. 10b and 10d) during major El Niños encompass the entire thermocline, while notable temperature changes can be followed down to 150 m depth (Figs. 10a and 10c). Wave propagation is not obvious in Fig. 10. The wind stress changes seem to be too gradual so that the model ocean is always in a state of quasi-equilibrium with the wind stress field.

7. The 1982/83 El Niño

The last El Niño event took place during the years 1982 and 1983. It was the strongest warm event reported in this century. Fortunately, this event is well observed and it is therefore suitable to make not only qualitative but also quantitative comparisons between the available data and the model results. Philander and Seigel (1985) have already performed a successful simulation of this event by forcing their ocean model with a different wind field. One deficiency of that simulation is the inability of the model to recover from El Niño conditions. One possible reason for this feature may be the quality of the wind field used, which is believed to be inaccurate. It is therefore of special interest to show a simulation of the 1982/83 El Niño using the dataset of Goldenberg and O'Brien, because the model used by Philander and Seigel is quite similar to the model under consideration. Figure 11 shows a longitude–time section of the zonal pseudo stress component along the equator for 1982 and 1983 calculated from the dataset of Goldenberg and O'Brien. The most

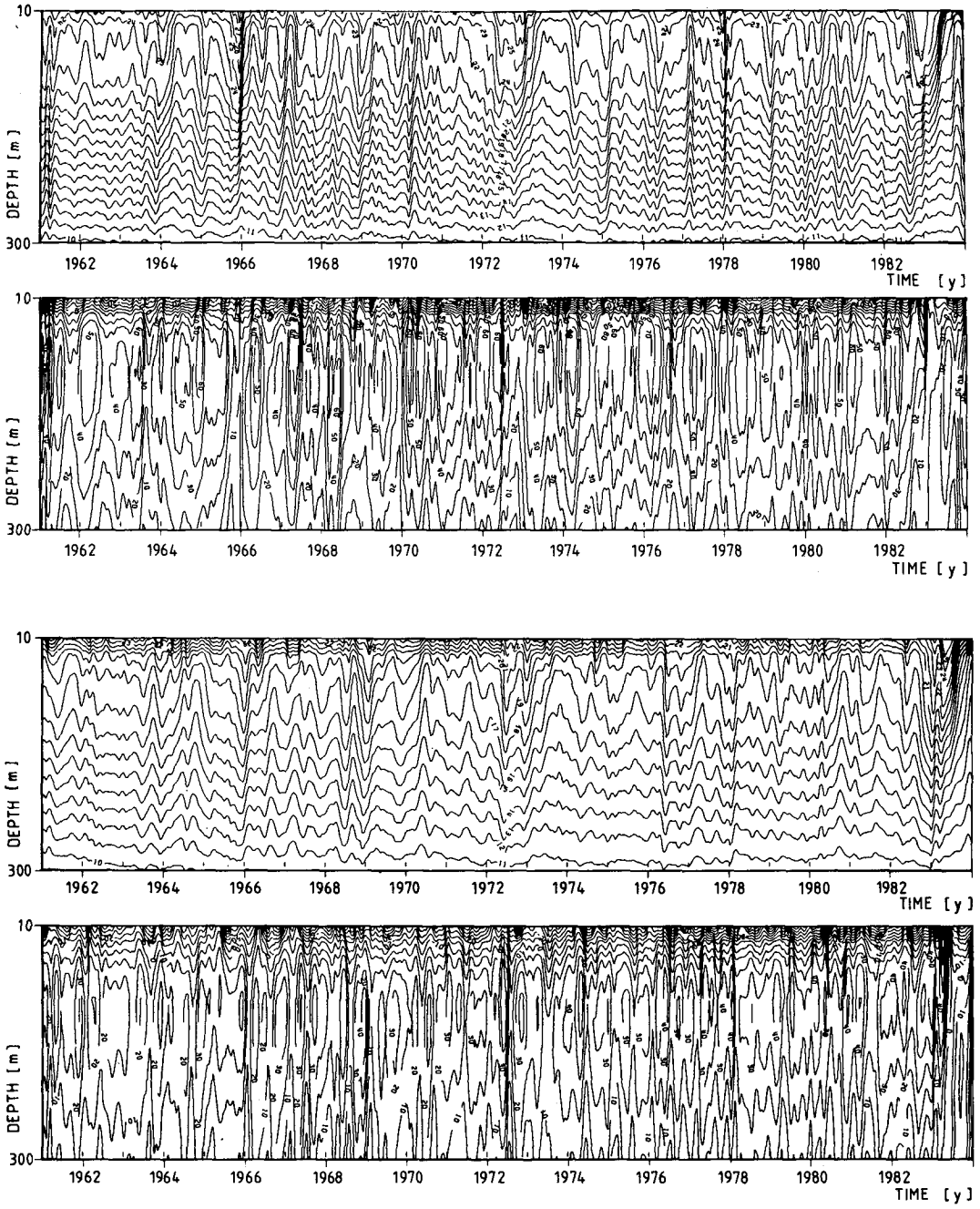

FIG. 10. Depth–time section of temperature (°C) (upper panel) at (a) 0°, 160°W, (b) zonal currents (cm s^{-1}) (lower panel) at 0°, 157°W, (c) temperature at 0°, 117°W and (d) zonal currents at 0°, 114°W.

prominent feature is the slow propagation of westerly winds from the western Pacific into the eastern Pacific. By about March 1983 the westerly winds have reached the eastern Pacific. At this time the trade winds have either reversed or are very weak along the entire equator. The trade winds remain weak until July 1983, while thereafter a gradual intensification of the trades is found. At the end of 1983 the recovery of the trade wind field is accomplished.

Longitude–time sections of temperature and zonal currents along the equator simulated by the model are shown for three different levels in Fig. 12. The evolution of sea surface temperature is presented in Fig. 12a. In early 1982 conditions are normal, showing warm water in the western and cold water in the eastern Pacific. The first significant change happened in March 1982, when a warming of about 2°C of the cold water pool took place. At about the same time westerly winds are

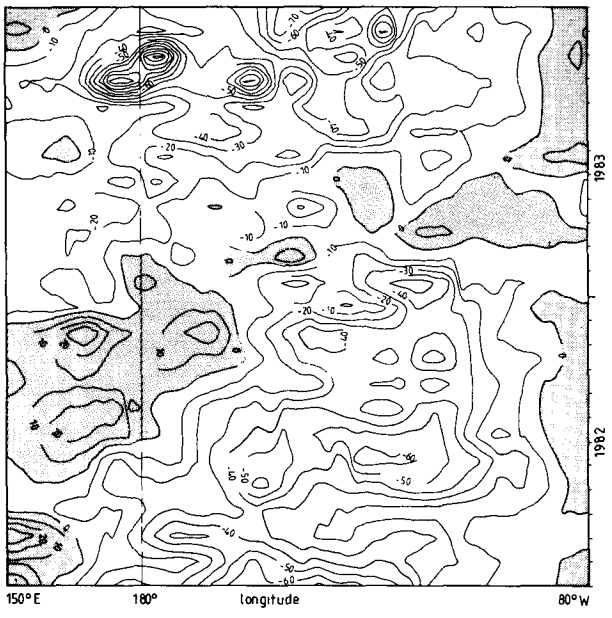

FIG. 11. Longitude–time section of zonal pseudo stress in units $m^2 s^{-2}$ during 1982/83 interpolated on the equator. Shaded area indicates eastward motion.

found in the western Pacific and the warm water west of the dateline starts to move eastward. While the western Pacific thereafter continues to warm up, sea surface temperatures in the east fall again reaching minimum values in June 1982. Zonal surface currents (Fig. 12b) also show pronounced variations up to this time. In the beginning of 1982 strong westward surface currents are found along the equator while weaker currents of less than 10 cm s^{-1} are simulated by the model in March 1982. This deceleration of the equatorial current coincides with the first warming in the eastern Pacific. From March to June 1982 a very strong eastward surface current developed west of the dateline. This might be regarded as the onset of El Niño. In the eastern Pacific there is found almost simultaneously an intensification of the westward surface current, which is associated with the previously discussed temperature minimum in June 1982. During the second half of 1982 the sea surface temperature increases in the eastern Pacific and remains high in the western Pacific. The occurrence of warm surface waters on the equator follows approximately the path of the westerly winds. By March 1983 the entire equator is covered with warm water resulting in an almost homogenous distribution of surface temperature. Zonal currents evolve in a similar manner. After June 1982 the westward flow starts to decelerate in the eastern Pacific, while currents remain eastward in the western Pacific. The expansion of eastward jets also follows the path of the westerly winds. The maxima of eastward surface flow coincide roughly with the extremes of the westerly winds. During March 1983 an intense eastward surface jet has developed, which covers the equator from the eastern coast to about 170°W. At this time the termination phase has already started in the western Pacific. As can be seen from Fig. 12b, surface currents west of the dateline are already westward. Sea surface temperatures (Fig. 12a) recover very quickly. The strong temperature fall starts in the vicinity of the dateline in June 1983 and propagates rapidly eastward. By August 1983 temperatures fall along the entire equator. At this time surface currents are already westward over the largest portion of the equator.

The evolution of zonal currents during the 1982/83 El Niño shows a remarkable agreement with the simulation of Philander and Seigel (1985). Particularly, the development of eastward surface jets during the second half of 1982 in the western Pacific, the occurrence of an eastward jet in spring 1983 in the eastern Pacific and strong westward flow in late 1983 west to the dateline are found in both simulations.

By December 1983 the trades are anomalously strong (Figs. 2 and 11). At the end of 1983 the model ocean has therefore reached a cold state accompanied by strong westward currents. Negative sea surface temperature anomalies during December 1983 exceed values of 2°C (Figs. 5b, 6b), while the observations indicate almost normal conditions (CAC 1983). As can be seen from Fig. 12a, the center of the cold water pool in the eastern Pacific shows temperatures down to 20°C.

Temperature and zonal current changes at a depth of 50 m are presented in Figs. 12c and 12d. The temperature at 50 m depth (Fig. 12c) evolve in a similar manner as the sea surface temperature. Warming starts again in the western Pacific and propagates eastward at about the same speed as at the surface. The occurrence of eastward jets can be seen also at a depth of 50 m (Fig. 12d). Three areas of moderate westward flow can be seen in Fig. 12d. Westward currents at 50 m are found in the eastern Pacific during 1982, in the western Pacific in early 1983 and in the second half of 1983 in the eastern part of the basin.

Figures 12e and 12f show longitude–time sections of temperature and zonal currents at 100 m depth. Temperature variations (Fig. 12e) are again similar to those presented already in Figs. 12a and 12c. Zonal currents at 100 m undergo strong variations during the 1982/83 El Niño. As can be see from Fig. 12f in the beginning of 1982 there is found a fully developed equatorial undercurrent. By September 1982 and January 1983 weak westward flow is found in the western Pacific, while in the eastern half of the basin an undercurrent is present until March 1983. Thereafter motion decelerates in the east. For almost the rest of the year 1983 currents remain very weak in the eastern Pacific, while eastward currents develop gradually from March 1983 on in the western Pacific. The strong wind pulse over the western Pacific during September and October 1983 finally initiate the development of a strong undercurrent along the entire equator.

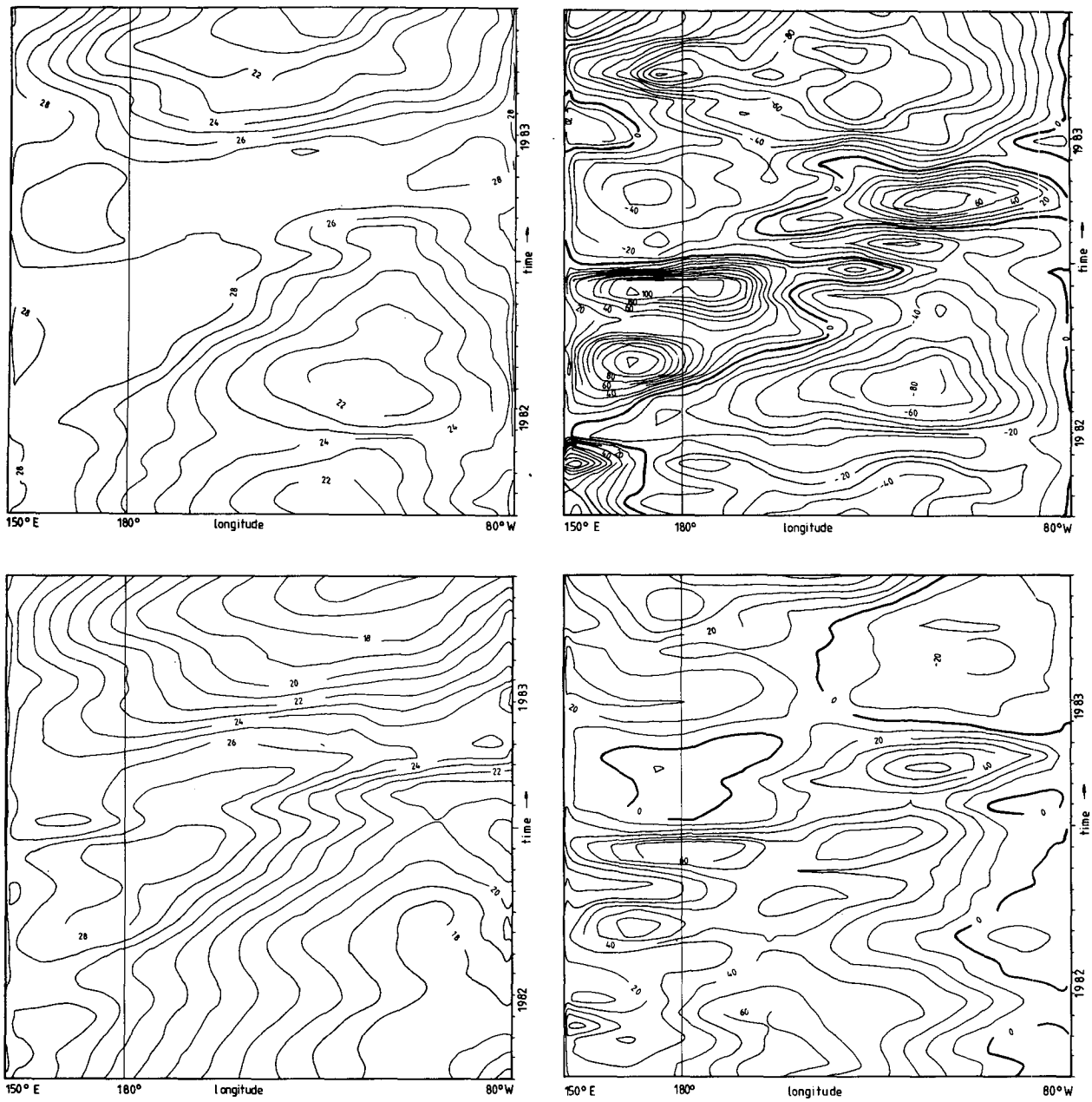

FIG. 12. Longitude–time sections along the equator for 1982/83 of temperature (°C) at (a) 10 m, (c) at 50 m, and (e) at 100 m and zonal currents (cm s^{-1}) at (b) 10 m, (d) at 50 m and (f) at 100 m.

Depth–time sections of temperature and zonal velocity on the equator are presented in Fig. 13. As can be seen from this figure the temporal and vertical structure of changes are so complicated that an interpretation in terms of a single wave mode is not possible.

The evolution of zonal currents on the equator at 157°W is shown in Fig. 13a. The corresponding measurements can be found in Firing (1983). As can be seen from Fig. 13a, in the first half of 1982 variations in the current structure are weak. The most prominent feature during this period is the intensification of the undercurrent in April 1982 associated with a deceleration of the westward surface current. This feature can also be found in more pronounced form in the measurements of Firing. After the surface current recovers for a short period in the model it starts to decelerate again in June. In November 1982 the model shows the existence of an intense eastward surface jet and weak

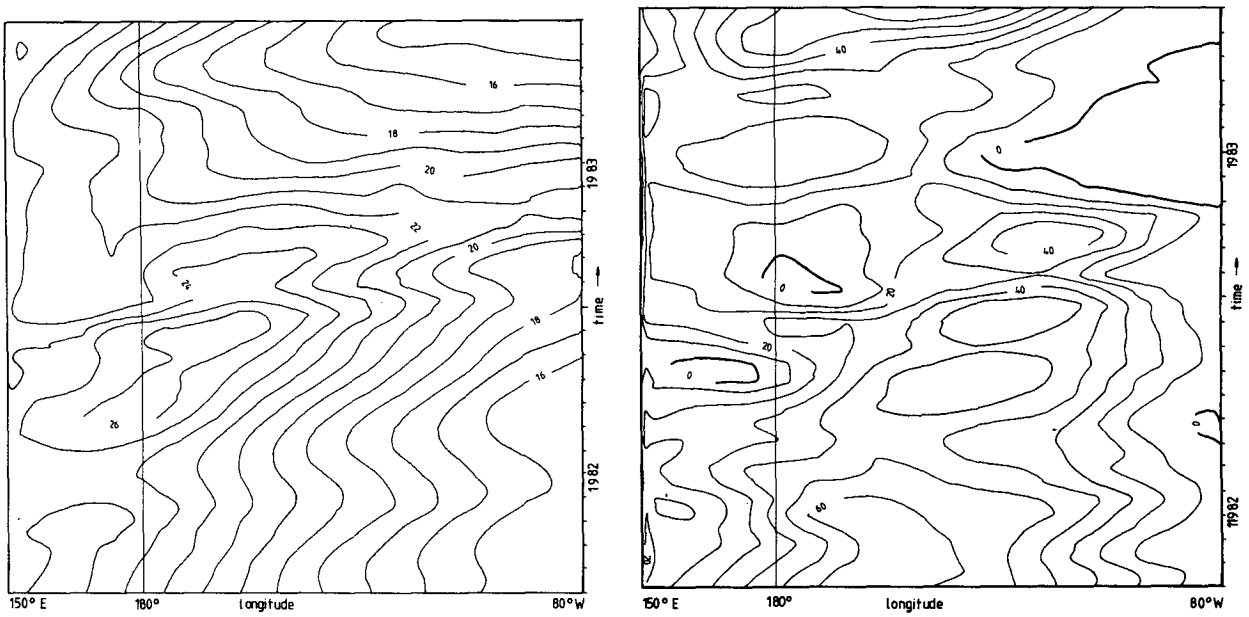

FIG. 12. (*Continued*)

subsurface currents. The observations show basically the same behavior. In December 1982 both simulation and observation indicate a very fast breakdown of this eastward surface jet. While almost normal conditions are found already in the measurements by March 1983, the recovery is delayed in the model, showing almost normal conditions from June 1983 on. The evolution of the thermal structure in the central Pacific is given in Fig. 13b. Maximum temperature at the surface coincides with the occurrence of the eastward surface jet in November and December 1982. From January to May 1983 temperatures decrease almost gradually while stronger cooling is found at the end of May 1983. Temperature changes are small until September, when a pronounced cooling is found in the model simulation.

The situation in the eastern Pacific is shown in Figs. 13c and 13d, while observed sections at 0°, 95°W can be found in Halpern (1983). The first pronounced deceleration of the model undercurrent takes place in December 1982. As can be seen from Fig. 13c westward flow below 150 m is found in January 1983, a feature which can be seen also in the observations presented by Halpern. Both, the simulation and the observations show for March and April eastward surface currents and a second deceleration of the undercurrent. By May 1983 westward flow is found throughout the upper 300 m in the model. Finally the westward surface currents intensify until September 1983 and then change only slowly for the rest of the year. The undercurrent starts to develop again in July and does not reach normal strength in the model until the end of the simulation. The evolution of the temperature field in the eastern Pacific as calculated by the model is presented in Fig. 13d. While upper isotherms show only one pronounced downward drop as can be seen by following the 25°C isotherms, deeper isotherms exhibit a double peak signature, as exemplified by the 20°C isotherm. Warmest surface waters appear during the period of intense eastward surface currents in March and April 1983. At deeper levels the warming phase is interrupted by an upward motion of isotherms in January and February 1983, leading to the double peak signature. By May 1983 at all levels the cooling phase has started resulting in a gradual shoaling of the thermocline, which lasts for the rest of the year.

The basinwide character of the 1982/83 El Niño event is demonstrated by Fig. 14, showing depth–longitude sections of temperature along the equator for three different times. As indicated by the 16°C-isotherm the position of the thermocline is quite normal by July 1982 (Fig. 14a). As can be seen from Fig. 11 this period is characterized by trade winds of normal strength. By April 1983 no tilt of the 16°C-isotherm is found (Fig. 14b). While the thermocline maintained almost its position in the western part of the basin, the 16°C-isotherm for example has been pushed down in the east by about 120 m. From Fig. 11 it can be seen that at this time zonal winds are rather weak along the entire equator. It was already seen in Fig. 13 that by April 1983 the undercurrent is weak in the central Pacific and has disappeared in the eastern Pacific. This behavior is consistent with the vanishing of the pressure force within the thermocline (Fig. 14b). By September 1983 isotherms tilt again upward in the eastern Pacific

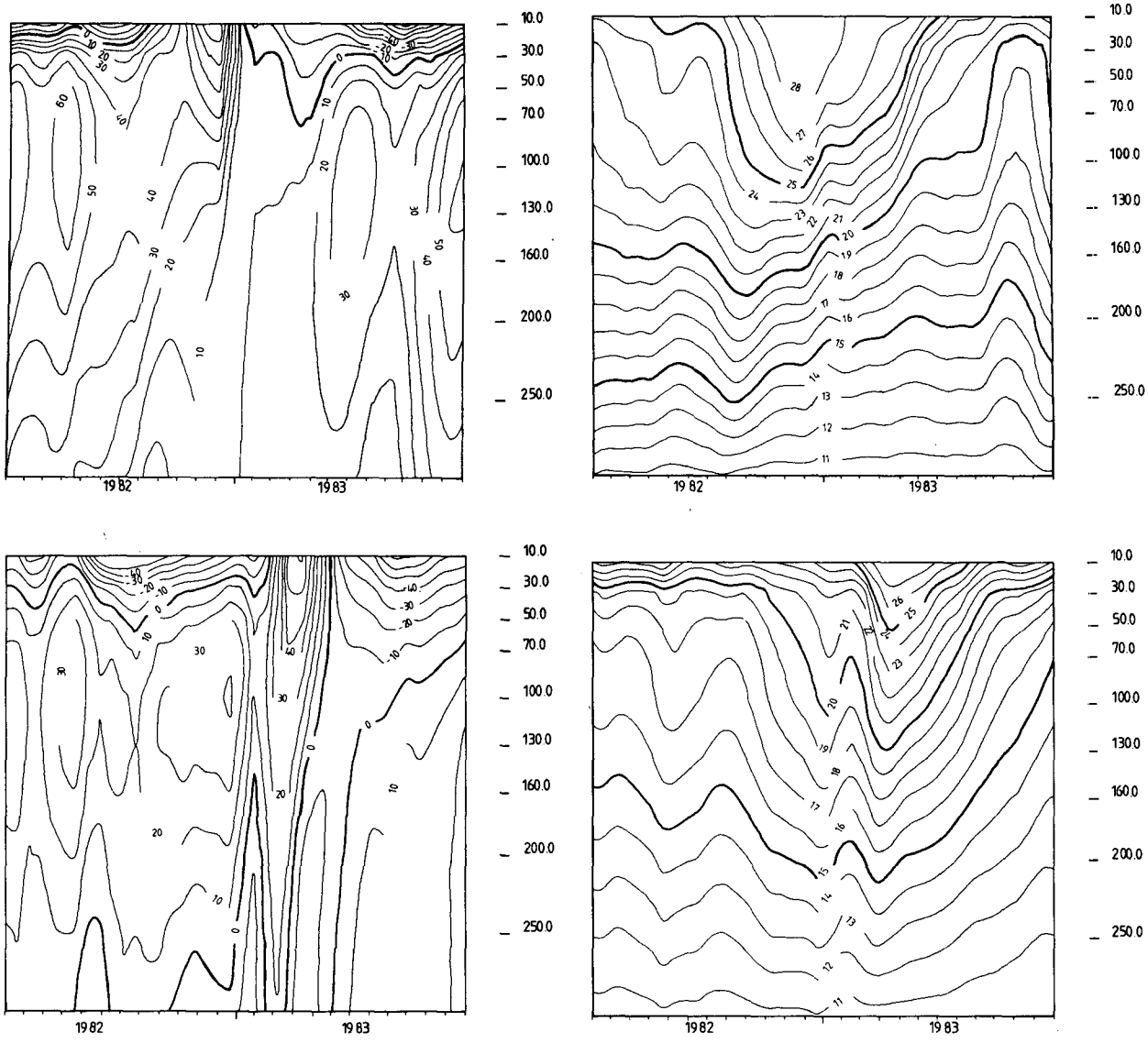

FIG. 13. Depth–time sections along the equator for 1982/83. Zonal currents (cm s^{-1}) at (a) 157°W and (c) 99°W and temperature (°C) at (b) 160°W and (d) 103°W.

(Fig. 14c) due to the intensification of the trades (Fig. 11). As can be seen from Fig. 12, the recovery of the ocean is not completed at this time so that the cold water pool at the surface is located too far west in Fig. 14c.

The meridional extent of current changes at 157°W is shown in Fig. 15. By September 1982 eastward currents start to develop reaching maximum strength in December 1982. At this time motion is eastward from 4°S to about 10°N. The center of the eastward jet is located slightly south of the equator. In January 1983 westward motion is found north of the equator, while eastward currents are still found south of the equator. This eastward current persists until May 1983. Thereafter pronounced westward motion is found between 5°S and 5°N and a weak counter current develops north of 5°N.

Quantitative comparisons of different variables with observed times series are presented in Fig. 16. The observations were taken from the paper of Halpern (1983). In Figure 16a near surface temperatures in the eastern Pacific are compared. As can be seen from Fig. 16a, temperatures start to increase as early as the second half of 1981. Both simulation and observation show a moderate temperature peak in early 1982. After a short decrease, the temperature increases again in July 1982 and reaches a maximum value in early 1983. The general evolution of simulated near surface temperatures

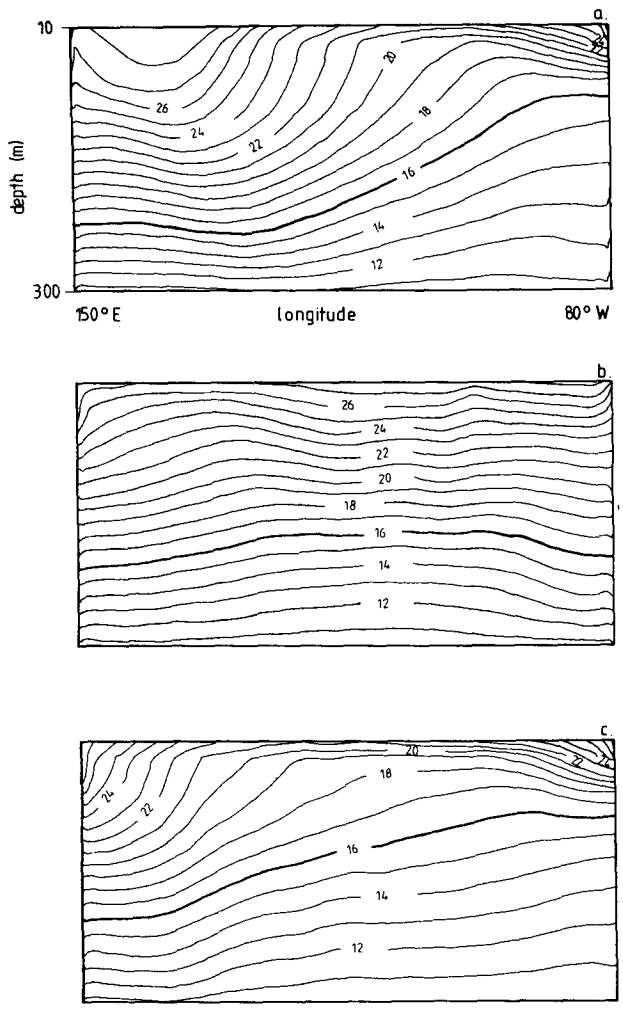

FIG. 14. Longitude–depth sections of temperature (°C) along the equator for (a) July 1982, (b) April 1983 and (c) September 1983.

agrees reasonably well with the observed time series, while month to month variability show considerable discrepancies among the two curves. The same kind of comparison is shown in Fig. 16b for temperatures at 100 m depth. The simulation as well as the observation exhibits only small variations until July 1982. While the observations show a sharp increase in temperature after July the simulation underestimates this rise. Also the sharp drop of temperature in January 1983 is visible in the model simulation only in less pronounced form.

Zonal currents within the upper 30 m are shown in Fig. 16c. The most prominent feature of the observed time series of zonal currents is the existence of a strong seasonal cycle prior to the El Niño event. This behavior can also be seen in the model time series at 10 m. The observed record of zonal currents is unfortunately not long enough to identify the evolution of the eastward surface jet in March 1983. Zonal currents at 100 m (Fig. 16d) are in general too weak in the model simulation and the first decrease by December 1982 is not as strong as in the observed time series. A comparison of changes in the heat content of the upper ocean in the eastern Pacific is presented in Fig. 17. The model shows slightly higher values of heat content during the whole time. This feature is due to the fact that integration of model temperature was carried out for a longer depth interval. The model times series reproduces reasonably well the observations. In both time series the first small peak in heat content is found in May 1982, the steady increase of heat content in the second half of 1982, and the drop in January 1983. As was already seen in Fig. 16b subsurface temperatures show less pronounced variations during this El Niño event. For this reason the increase in heat content from July to December 1982 is less steep in the model.

The relative roles of the different terms in the temperature equation at the surface are shown in Fig. 18a for a location of 175°W, 0°. As can be seen from Fig. 18a, prior to the El Niño event the model shows mainly a balance of surface heat flux and vertical advection of heat. In the beginning of 1982 both terms start to become smaller and the temperature at this location rises slowly. By July 1982 surface heat flux and vertical advection of heat have considerably diminished. At this time horizontal advection of heat, both zonal and meridional advection, are the largest terms in the temperature balance and the temperature shows a sharp increase. The occurrence of an eastward jet (Fig. 12) on the equator is associated with convergent motion

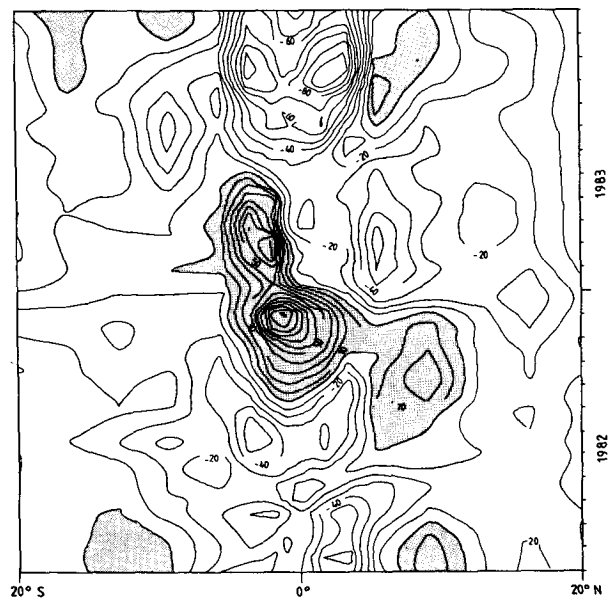

FIG. 15. Latitude–time section of zonal currents (cm s^{-1}) for 1982/83 at 157°W for a depth of 10 m. Shaded area indicates eastward motion.

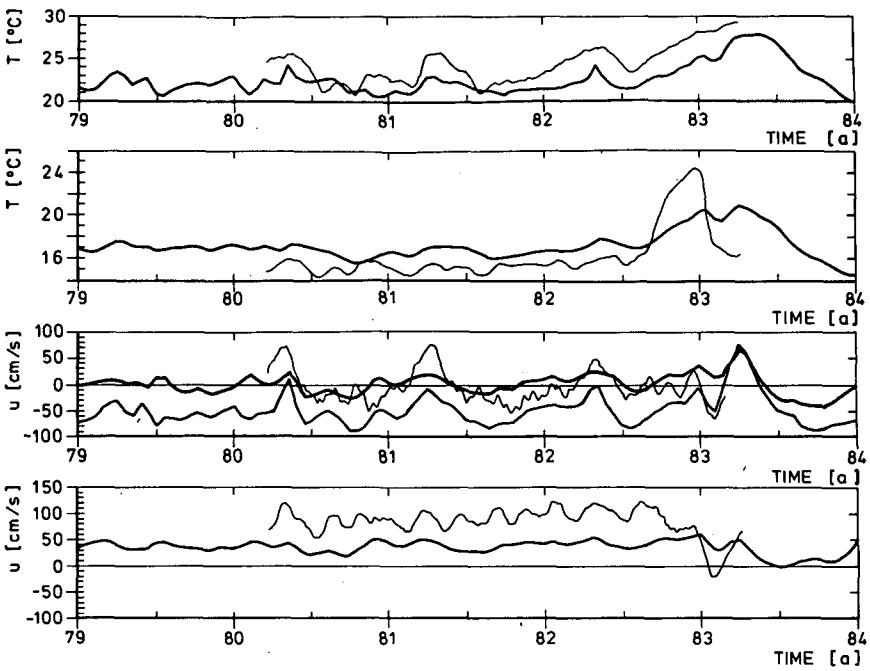

FIG. 16. Time series of temperature and zonal currents on the equator in the eastern Pacific. (a) Observed temperature (thin line) at 109°W and 15 m and computed temperature (thick line) at 117°W and 10 m, (b) observed temperature (thin line) at 109°W and 100 m and computed temperature (thick line) at 117°W and 100 m, (c) observed zonal currents (thin line) at 109°W and 15 m, computed zonal currents (medium line) at 114°W and 10 m and computed zonal currents (thick line) at 114°W and 30 m, (d) observed zonal currents (thin line) at 109°W and 100 m and computed zonal currents (thick line) at 114°W and 100 m. Observations were taken from Halpern (1983).

on both sides of the equator. This equatorward motion also tends to increase the temperature because it carries warmer water with it. At this time weak downwelling is found additionally. This situation remains almost unaltered for the rest of the year. In the beginning of 1983 the trades begin to recover in the western Pacific and the balance of surface heat flux and upwelling becomes again more important. For comparison the balance during the 1972 El Niño is given in Fig. 18b. During this event the warming evolved in a similar manner, except that the duration of anomalous conditions is about one year. As can also be seen from Fig. 18a and 18b during cold events (late 1973, late 1983) vertical advection of heat is responsible for the cooling.

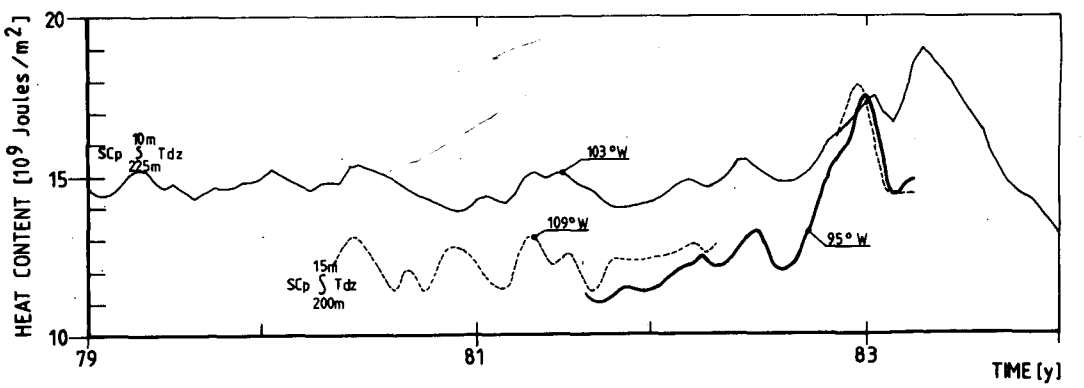

FIG. 17. Time series of heat content in the eastern Pacific, derived from observations (dashed and thick line) by Halpern (1983) and calculated by the model at 103°W (thin line).

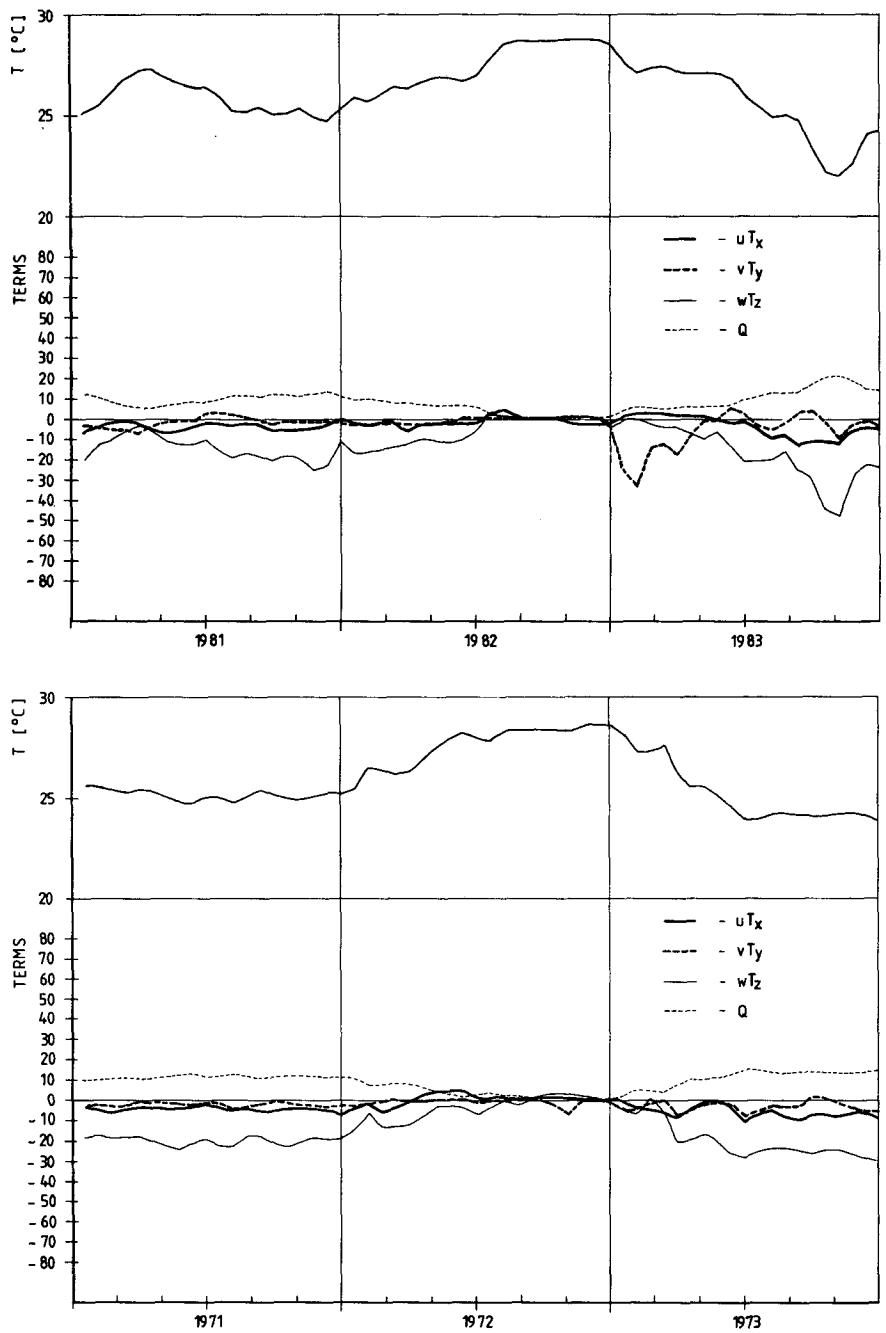

FIG. 18. Evolution of different terms (10^{-7} °C s^{-1}) of the temperature equation at 175°W, 0° (a) during the 1982/83 El Niño event and (b) during the 1972/73 event. Upper panels show in both figures the evolution of temperature during the El Niño periods.

8. Summary

The performance of a general circulation model of the tropical Pacific with respect to interannual variability is investigated. Three main subjects are addressed in this study: First, the importance of accurate estimates of wind stress for tropical ocean circulation experiments. Second, the ability of the model in reproducing observed low frequency changes of various ocean indices over decades. And finally, the evolution of the 1982/83 El Niño event.

The sensitivity experiment, which was performed by using two differently analyzed wind fields to force the ocean model (section 5) demonstrates that, espe-

cially in the eastern Pacific model, results depend strongly on the choice of wind field. As can be seen from Figs. 1 and 2, zonal wind stress anomalies in the eastern Pacific show little correspondence among the two datasets. Consequently the evolution of sea surface temperature anomalies in the eastern Pacific is very different from one model run to the other. The model results demonstrate that the random component of the wind field is important for tropical ocean circulation experiments in the eastern part of the Pacific, even if these fluctuations cannot be classified in a strictly statistical sense.

In the western Pacific the characteristics of the two wind fields are very similar (Figs. 1, 2, 3). Model results in the western Pacific show no basic differences between the two experiments.

In both simulations sea surface temperature variability in this region is modeled with some success. It is shown that the success of the model is not surprising because observed variations of sea surface temperature can be explained by a simplified model with no dynamics.

The investigation of interannual variability showed that the basic features of low frequency variability in the tropical Pacific can be reproduced by the model. Sea level variations along the equator compare reasonably well with the observed changes (Figs. 7a, 7b), showing opposite changes in the eastern and western parts of the basin. El Niño events are accompanied by lower than normal sea level in the western and higher than normal sea level in the eastern Pacific. Temperature and currents (Figs. 8, 9, 10) indicate a massive transfer of warm surface water from west to east during El Niño events. Typical values of eastward surface current anomalies during warm events are between 50 and 100 cm s^{-1}. Current changes are not only confined to the surface. At deeper levels the undercurrent also shows pronounced variations of about the same intensity as the surface currents. El Niño events are accompanied by a weaker than normal undercurrent. In a few cases surface currents can even reverse their direction.

These common features of El Niño events are most pronounced during the 1982/83 event. The model predicts sea surface temperature anomalies of more than 4°C in the eastern Pacific (Fig. 8b) and current anomalies of over 100 cm s^{-1} along the equator (Figs. 9a, 9b). As can be seen from Figs. 12 and 15, strong eastward surface currents transfer warm water into the eastern Pacific. It is shown that during El Niño events the temperature balance changes completely. While before and after El Niño events the model shows mainly a balance between vertical advection of heat and surface heat flux, during the warm period all three advective terms are of the same order of magnitude and zonal advection of heat becomes the largest term. Another pronounced observed feature of the 1982/83 events is the deceleration of the undercurrent, which is simulated in less pronounced form by the model. This deceleration is accompanied by basinwide changes of thermocline depth (Fig. 14), which shows temporarily an almost horizontal position. The eastward flux of warm water at 100°W as calculated from the model results amounts to 36×10^6 m^3 s^{-1} through a plane defined by 12°S to 12°N and the upper 275 m.

As was shown in Latif et al. (1985), the model in its present version yields a very poor representation of the mean state and the seasonal cycle. The currents, for example, are much too weak, especially in the eastern part of the basin. While observations indicate values of the undercurrent in the eastern Pacific up to 100 cm s^{-1} and even more (Halpern 1983), in the model simulation the speed of the undercurrent is only about one third of the observed value. Another model flaw is the absence of a sharp thermocline in the model. As was shown by Pacanowski and Philander (1981) these two shortcomings of the model could be overcome by using nonconstant values of vertical eddy viscosity and diffusivity.

The mean horizontal pattern of sea surface temperature also shows big differences from the observations. The model cannot produce the characteristic meridional distribution of temperature because there is no meridional flux at of temperature at the surface through the northern and southern boundaries. Therefore, the model shows only the two upwelling regions along the equator and the southeastern boundary, while in all other regions the surface temperature is more or less equal to the forcing temperature of 29°C. There are at least two possibilities to improve the SST climatology in the model. One way is to use open boundary conditions. Another way would be to force the model with nonuniform air temperatures. Although the model must be improved with respect to the mean state and seasonal variations, it seems to be possible to simulate realistic low-frequency variations.

Therefore, work is now in progress to develop a coupled ocean–atmosphere model consisting of the ocean model presented in this paper and a fully prognostic primitive equation global atmosphere model. The aim of this future project is to test if complete El Niño cycles can be predicted with a coupled general circulation model run in a fully interactive mode.

Acknowledgments. The author appreciates very much the support of Drs. T. P. Barnett and J. J. O'Brien for making the wind datasets available. I like to thank very much Dr. D. Olbers for many fruitful discussions and Dr. E. Maier-Reimer for providing the model.

Special thanks to Mrs. M. Grunert for preparing the figures and Mrs. U. Kircher for typing the manuscript.

REFERENCES

Barnett, T. P., 1983: Interaction of the monsoon and Pacific trade wind system at interannual time scales. Part I: The equatorial zone. *Mon. Wea. Rev.*, **111**(4), 756–773.

Bryan, K., 1969: A numerical method for the study of the circulation of the ocean. *J. Comput. Phys.*, **4**, 347–376.

Busalacchi, A. J., and J. J. O'Brien, 1981: Interannual variability of the equatorial Pacific in the 1960's *J. Geophys. Res.*, **86**(11), 10901–10907.

——, K. Takeuchi and J. J. O'Brien, 1983: Interannual variability of the equatorial Pacific. *Hydrodynamics of the Equatorial Ocean.* J. C. J. Nihoul Ed., Elsevier Oceanogr. Ser., Vol. 36.

CAC, 1986, Climate Diagnostics Bulletin (Feb. 1986). Climate Analysis Center, Washington, DC 10233.

Cane, M. A., 1979a: The response of an equatorial ocean to simple wind stress patterns: I. Model formulation and analytic results. *J. Mar. Res.*, **37**, 232–252.

——, 1979b: The response of an equatorial ocean to simple wind stress patterns: II. Numerical results. *J. Mar. Res.*, **37**, 253–299.

——, 1984: Modelling sea level during El Niño. *J. Phys. Oceanogr.*, **14**, 1864–1874.

Firing, E., 1983: Currents in the central equatorial Pacific during the 1982–83 El Niño. Papers from 1982/83 El Niño/Southern Oscillation Workshop. NOAA/AOML, Miami, Florida.

Gill, A. E., 1983: An estimation of sea level and surface current anomalies during the 1972 El Niño and consequent thermal effects. *J. Phys. Oceanogr.*, **13**, 586–606.

——, and E. M. Rasmusson, 1983: The 1982–83 climate anomaly in the equatorial Pacific. *Nature*, **306**(5940), 229–234.

Goldenberg, S. O., and J. J. O'Brien, 1981: Time and space variability of tropical pacific wind stress. *Mon. Wea. Rev.*, **109**, 1190–1207.

Halpern, D., 1983: Upper ocean current and temperature observations along the equator west of the Galapagos Islands before and during the 1982–83 ENSO event. Papers from 1982/83 El Niño/Southern Oscillation workshop. NOAA/AOML, Miami, Florida.

Haney, R. L., 1971: Surface thermal boundary condition for ocean circulation models. *J. Phys. Oceanogr.*, **1**, 241–248.

Horel, J. D., and J. M. Wallace, 1981: Planetary-scale atmospheric phenomena associated with the Southern Oscillation. *Mon. Wea. Rev.*, **109**, 813–829.

Hurlburt, H. E., J. C. Kindle and J. J. O'Brien, 1976: A numerical simulation of the onset of El Niño. *J. Phys. Oceanogr.*, **6**, 621–631.

Latif, M., E. Maier-Reimer and D. J. Olbers, 1985: Climate variability studies with a primitive equation model of the equatorial Pacific. *Coupled Ocean–Atmosphere Models*, J. C. J. Nihoul, Ed., *Elsevier Oceanogr. Ser.*, Vol. 40.

McCreary, J., 1976: Eastern tropical ocean response to changing wind systems: With application to El Niño. *J. Phys. Oceanogr.*, **6**, 632–645.

Meyers, G., 1979: Annual variation in the slope of the 14°C isotherm along the equator in the Pacific Ocean. *J. Phys. Oceanogr.*, **9**, 885–891.

Pacanowski, R. C., and S. G. H. Philander, 1981: Parameterization of vertical mixing in numerical models of tropical oceans. *J. Phys. Oceanogr.*, **11**, 1443–1451.

Philander, S. G. H., 1981: The response of equatorial oceans to a relaxation of the trade wind field. *J. Phys. Oceanogr.*, **11**, 176–189.

——, and R. C. Pacanowski, 1980: The generation of equatorial currents. *J. Geophys. Res.*, **85**, 1123–1136.

——, and ——, 1981: Response of equatorial oceans to periodic forcing. *J. Geophys. Res.*, **86**(C3), 1903–1916.

——, and A. D. Seigel, 1985: Simulation of El Niño of 1982–1983. Coupled ocean–atmosphere models. J. C. J. Nihoul, Ed., *Elsevier Oceanogr. Ser.*, Vol. 40.

Rasmusson, E. N., and T. H. Carpenter, 1982: Variations in tropical sea surface temperature and surface wind fields associated with the Southern Oscillation/El Niño. *Mon. Wea. Rev.*, **10**, 354–384.

Robinson, M. K., 1976: *Atlas of North Pacific Ocean, Monthly Mean Temperature and Mean Salinities of the Surface Layer.* Naval Oceanographic Office, Ref. Publ. 2, Washington, DC.

Wright, P. B., 1977: The Southern Oscillation-patterns and mechanisms of the teleconnections and the persistence, HIG-77-13, Hawaii Inst. of Geophys., University of Hawaii.

Wyrtki, K., 1974: Equatorial currents in the Pacific 1950 to 1970 and their relations to the trade wind field. *J. Phys. Oceanogr.*, **4**, 372–380.

——, 1975: El Niño—The dynamic response of the equatorial Pacific ocean to atmospheric forcing. *J. Phys. Oceanogr.*, **5**, 572–584.

——, and G. Meyers, 1975a: The trade wind field over the Pacific Ocean. Part I: The mean field and the annual variation. Rep. HIG-75-1. Hawaii Inst. Geophys., University of Hawaii, Honolulu, Hawaii, 26 pp.

——, and ——, 1975b: The trade wind field over the Pacific Ocean. Part II: Bimonthly fields of wind stress; 1950 to 1972. Rep. HIG-75-2. Hawaii Inst. Geophys., University of Hawaii, Honolulu, Hawaii, 16 pp.